Performance Indexes Evaluation of a Novel Synchronous Reluctance Motor with Sinusoidal Rotor Shape

SCHOLARONE™
Manuscripts

Dear Editor-in-chief

The paper titled "Performance Indexes' Evaluation of a Novel Synchronous Reluctance Motor with Sinusoidal Rotor Shape" was submitted to the IEEE Transactions on Magnetics on October 15, 2017. A response from the journal editor-in-chief came on October 21, 2017 to notify that the paper is out their scope. The official response from the IEEE Transaction on Magnetics is attached to this cover letter.

Kind Regards,

DR. M. MUTEBA

Decision Letter (TMAG-17-10-0742)

From:	kabos@boulder.nist.gov
To:	mmuteba@uj.ac.za, mbika71@gmail.com
CC:	
Subject:	Transmag: Manuscript submission -- TMAG-17-10-0742
Body:	Dear Dr. MUTEBA:

Unfortunately we are unable to accept the paper listed below, which you submitted on the IEEE Transactions on Magnetics ScholarOne Manuscripts Web site, because it does not fall sufficiently within the current regular scope of our publication. We suggest you consider submitting it to IEEE Transactions on Industry Applications, for which it is better suited.

While we regret not being able to accept your manuscript, we thank you for sending it to us for consideration and hope that our prompt decision will enable you to pursue other ways to disseminate your results in a timely manner. We apologize for any inconvenience.

Sincerely,
Pavel Kabos
Editor-in-Chief
IEEE Transactions on Magnetics

Manuscript Title: Performance Indexes' Evaluation of a Novel Synchronous Reluctance Motor with Sinusoidal Rotor Shape
ID: TMAG-17-10-0742

Date Sent: 21-Oct-2017

     ☒ Close Window

Performance Indexes' Evaluation of a Novel Synchronous Reluctance Motor with Sinusoidal Rotor Shape

M. Muteba, *Member, IEEE*, B. Twala, *Member, IEEE*, and D. V. Nicolae, *Member, IEEE*

Abstract— **This paper presents the evaluation of performance indexes of a novel Synchronous Reluctance Motor (SynRM), which has an axially sinusoidal rotor lamination shape. The stator of a 5.5 kW, 4-pole, 50 Hz conventional three-phase squirrel cage induction motor, with distributed and chorded by one slot, double layer winding, is used for both standard and novel synchronous reluctance motors. Due to the nature of the sinusoidal rotor structure, the 3D Finite Element Analysis (FEA) is utilized to study the electromagnetic parameters of interests. The SynRM with sinusoidal rotor shape results are compared with the standard SynRM without cut-off on the *q*-axis. The FEA results are validated by means of practical measurements. From both FEA and measured results, it is evident that the novel SynRM enhances the performance indexes of interests such as torque density, torque ripple factor and efficiency.**

Index Terms— **Enhanced performance indexes, high torque density, low torque ripple, novel rotor with sinusoidal shape, synchronous reluctance motor**

I. INTRODUCTION

THE Synchronous reluctance machines (SynRMs) are good competitors in AC drives due to their compact design and high power density. They have also become an interesting choice, being used as small power motors in various applications [1]. One of these applications is a small electric scooter, commonly used by people with physical disabilities. In [2] the in-wheel switched reluctance motor driving system for future electric vehicles (EVs) has been reported. A mechanical robust rotor with transverse-laminations for a synchronous reluctance machine for electric traction application is discussed with more details in [3]. The novel lamination concept for transverse flux machines suitable for direct drive application to EVs is presented in [4]. The design optimization of SynRM drives for Hybrid Electric Vehicles (HEVs) power train application is analyzed in [5].

However, the interaction between spatial harmonics of the electrical loading and the rotor anisotropy of SynRMs causes a high torque ripple that is intolerable in most applications [6], [7]. A good number of previous work intended to reduce the torque ripple contents in SynRMs, directing their focus mostly to a suitable choice of number of flux-barriers in respect to the number of stator slots per pole per phase [8], [9], the optimization and asymmetry of the flux-barriers geometry, etc., [7], [10], [11], [12], [13].

In 2014, Zhao proposed and analyzed the material-efficient Permanent Magnet Synchronous motor with a sinusoidal magnet shape [14].

The analysis was performed on fraction of Horse power (Hp) permanent magnet surface-mounted motors used in automotive actuators. For a total rotor volume of 86.6 cm^3, the magnet volume of 18.2 cm^3 for the proposed Permanent Magnet Synchronous motor with sinusoidal magnet shape was obtained [14]. Although, both Finite Element Analysis (FEA) and practical results presented by Zhao are satisfactory, the use of the proposed motor is limited to a fraction of Hp application. For medium and high power motors to be used in traction, electric vehicles and hybrid electric vehicles, where less torque ripple and high torque density are required, the magnet volume will be intolerably high.

The novel SynRM with sinusoidal rotor shape in the axial direction, without changing the flux barrier geometry has positioned itself as an alternative in applications that require high torque density and less torque ripple. The novel motor was first reported in 2016 [15]. The study was done on 1.5 kW, six-pole machine and it was only limited to FEA [15].

In this paper the performance indexes of the Novel SynRM with a sinusoidal rotor lamination shape in the axial direction are evaluated, and compared to a standard SynRM of the same ratings.

II. NOVEL MOTOR GENERAL SPECIFICATIONS

Fig.1 (b) illustrates the cross-section of basic SynRM with cut-off on *q*-axis, while Fig 1 (a) shows the photograph of the prototype for the standard rotor without cut-off on the *q*-axis. Table 1 depicts the general design specifications for a 4-pole, 5.5 kW SynRM with 36 stator slots.

The cross-section, the 3D view and the photographs of the prototype novel rotor with sinusoidal rotor shape are shown in Fig.2. The proposed novel rotor consists of stack laminations with identical flux barriers and different cut-off specifications on the *q*-axis. From Fig. 2, it is noted that the variation of the cut-off pitch angle results in step-changing of the cut-off base lengths, thus forming a sinusoidal shape along the axial length of the rotor. It should also be noted that the middle stack lamination shape has no cut-off angle at all and isolates the two adjacent periodical structures
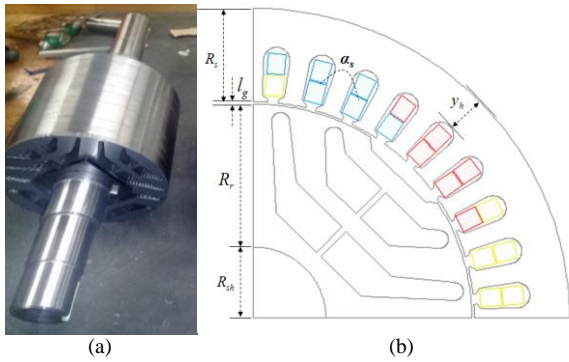
Fig.1: Standard SynRM, (a) Photograph of the prototype rotor without cut-off, (b) cross section of the standard SynRM with cut-off on the *q*-axis

TABLE I
GENERAL DESIGN SPECIFICATIONS

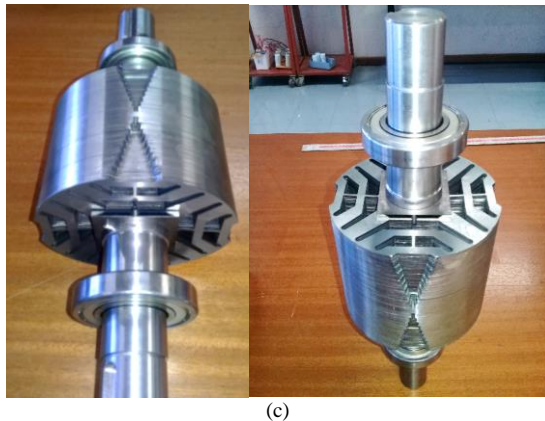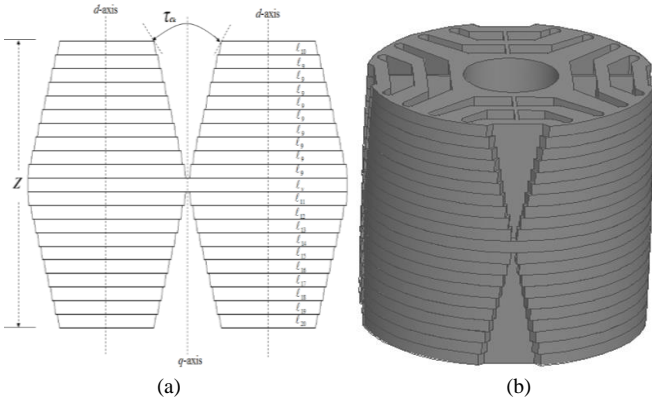| Description	Values
Stator slot α_s	10° mech
Airgap length l_g	0.88 mm
Stack length Z	160 mm
Number of barriers per pole	2
Number of pole pairs p	2
Number of stator slots Q_s	36
Rotor radius R_r	48.80 mm
Stator radius R_s	31.62 mm
Shaft radius R_{sh}	24.00 mm
Yoke height y_c	12.87 mm

Fig. 2: Rotor of the Novel SynRM, (a) cross-section, (b) 3D view, (c) photographs of the prototype novel SynRM rotor

III. FINITE ELEMENT ANALYSIS

A. Finite Element Method

For 2D magnetic field, the magnetic potential has only no-zero component along the Z-axis, thereby reducing the computation effort by order of magnitude [16]. Due to the axial geometry design of the Novel SynRM, a three-dimensional (3D) Finite Element Analysis (FEA) is performed in this paper, using ANSYS 16.0 electromagnetic package. The flux density distribution and the inductances are numerically computed through the magnetostactic solver. A bounded domain $V = V_1 + V_2 + \dots + V_n$ of the 3D space is considered and the equations that characterised the magnetostatic problem in domain V are illustrated in [17]. For the Novel SynRM, the magnetic vector potential is not constant along the transverse cross-section because of the reluctance variation in the axial direction of the airgap. The leakage flux of coils placed in stator slots will not be the same. The Kelvin-Stokes expression applied to the closed contour of the airgap of the Novel SynRM in 3D space with bounding a volume V is obtained by using the superposition principle and is written as [18]

$$\iint_{\Omega_1} \nabla \times A_1 \cdot d\Delta g_1 + \dots + \iint_n \nabla \times A_n \cdot d\Delta g_n$$
$$= \iiint_{V_1} \nabla \times A_1 \cdot dV_1 + \dots + \iiint_{V_n} \nabla \times A_n \cdot dV_n \quad (1)$$

Where ∇ is a vector operator, A is the magnetic vector potentials, Δg is the airgap area and the subscript "*n*" represents the number of the corresponding stack rotor lamination. In total, 380 SURA M400-50A lamination sheets are used to constitute 21 stack rotor laminations of the prototype rotor core shown in Fig 2. On the other hand, Fig.3 shows the mesh plot on the surface of the rotor of the Novel SynRM with sinusoidal rotor shape (only one eighth of the rotor is shown). A total number of 18076 tetrahedral elements are obtained for the rotor geometry with minimum edge length of 0.007857 *mm* on the low magnetic reluctance pole face (*d*-axis region), and with maximum edge length of 16.4495 *mm* on the high magnetic reluctance pole face (*q*-axis region). The efficiency, power factor, flux-linkages and torque are obtained by using the magnetic-transient solver.
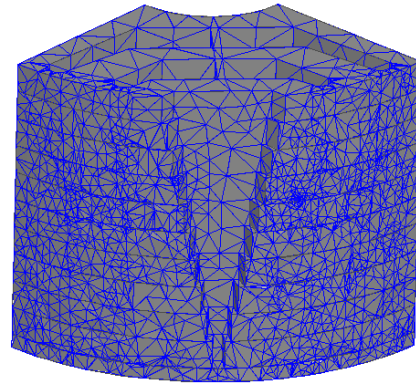

Fig. 3: Mesh plot of the rotor at full-load for the Novel SynRM

B. *Flux density distribution*

Only one eighth of the machine is modelled in order to reduce the computation time, Fig.4 shows the magnetic flux density distribution at full load plotted along the rotor periphery of the Novel SynRM. On other hand Fig. 5 shows the 3D airgap flux desity distribution on *d*-and *q*-axis of the Novel SynRM, and their average FFTs.
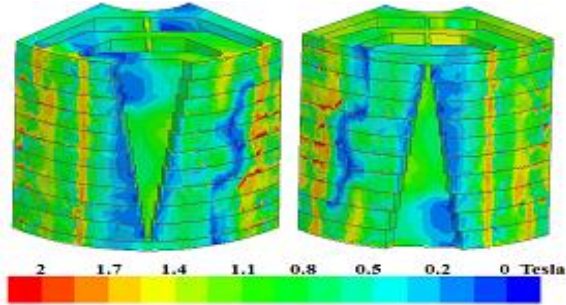

Fig. 4: Airgap flux density distribution on the rotor periphery of the Novel SynRM

From Fig.4 it is noticed that the *q*-axis current affects the flux density istribution. The analysis of *d*-axis and *q*-axis magnetic fields are done by exciting the stator three-phase winding by dc currents, with the rotor at standstill. The *dq*-axis magnetic field model of the machine is chosen to be 2D, with assumption of neglected end leakage and fringing effects, in order to save the computation time.

The Novel SynRM has a sinusoidal rotor shape in the axial direction, without changing the flux barrier geometry. As detailed in [18], the proposed novel machine consists of different laminations having different cut-off pitch angles near the airgap along the *q*-axis, thus forming a sinusoidal shape along the axial length of the rotor. Each lamination stack is modeled in 2D and the individual magnetic fields are superposed along the Z-length to obtain a 3D flux distribution representation. It is noted that the stator slotting affects the airgap density distribution in both *d*-and *q*-axis. However, the non-uniformed distribution of airgap density on *q*-axis due to variation of lamination shape along the stack length is very noticeable and significant. Fig.6 shows the superposed radial airgap flux density of the Novel SynRM.

Observing from the FFT results in Fig. 6 (b), it can be noticed that besides the fundamental component, there is a presence of odd ordinal numbers. The 19th harmonic has the highest amplitude after the fundamental. Those odd harmonics are caused not only by the distributed double layer winding itself but also by stator slotting, rotor cut-off openings and rotor flux barriers geometries. The 17th, 19th, 35th and 37th account for the stator slotting while the 11th, 13th, 23rd, 25th, 29th and 31st are due to rotor cut-off openings and flux barrier geometries. The 3rd and its multiples are mainly due to magnetic saturation. The presence of additional harmonics in the radial components of the airgap flux density results in the increase amount of the iron losses and thus decreased the efficiency [19].
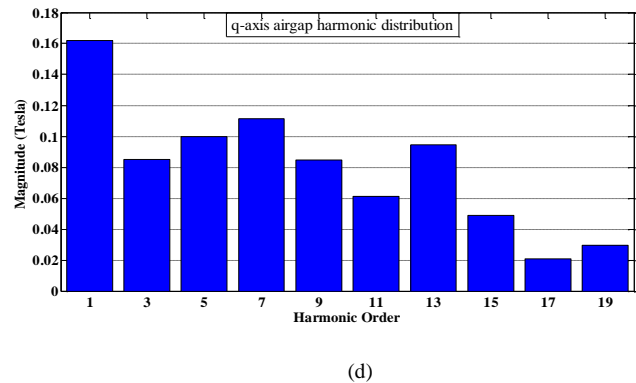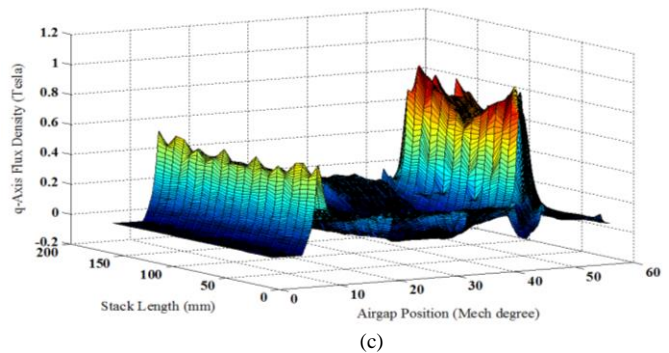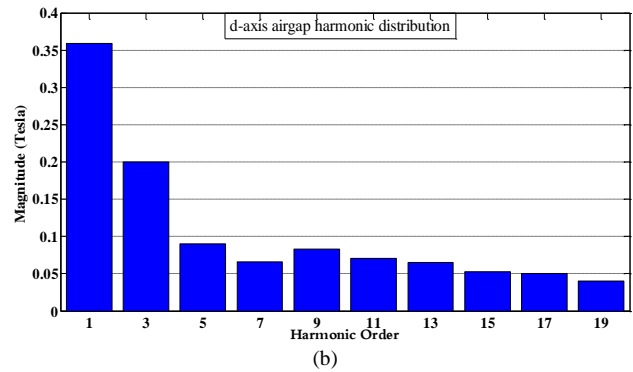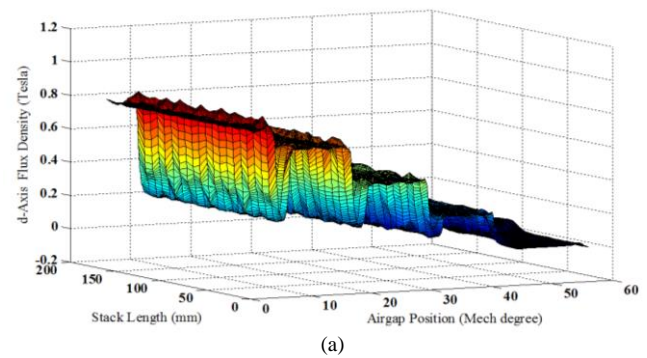

(a)

(b)

(c)

(d)

Fig. 5: *D*-axis and *q*-axis airgap flux density distribution, (a) 3D *d-axis* airgap profile, (b) FFT of the *d-axis* airgap flux density profile, (c) 3D *q-axis* airgap flux density profile, (d) FFT of the *q-axis* airgap flux density profile
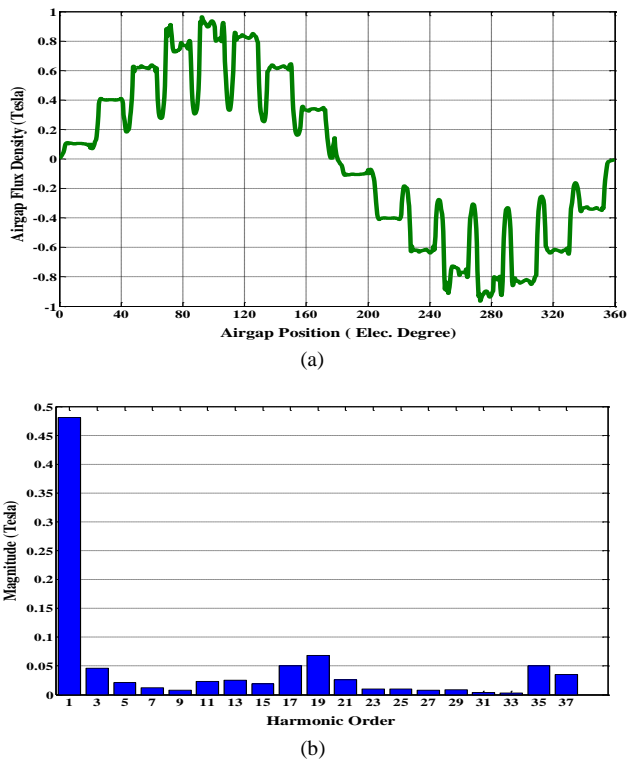
(a)

(b)

Fig.6: Superposed radial flux density distribution, (a) Flux density profile, (b) FFT of the flux density profile

C. Flux linkages

In the proposed Novel SynRM model, the cut-off pitch angle is varied along the q-axis, therefore changing quantities in the rotating reference frame. The stator flux linkages λ_a, λ_b and λ_c can be directly obtained from FEM. These stator flux linkages are converted into the rotating reference frame. The rotor quantities λ_d, λ_q and λ_o are given by [15]

$$\lambda_d = \frac{2}{3}\left[\lambda_a \cos\theta + \lambda_b \cos(\beta - 120) + \lambda_c \cos(\beta + 120^o)\right] \quad (2)$$

$$\lambda_q = -\frac{2}{3}\left[\lambda_a \sin\theta + \lambda_b \sin(\beta - 120^o) + \lambda_c \sin(\beta + 120^o)\right] \quad (3)$$

$$\lambda_o = \frac{1}{3}\left(\lambda_a + \lambda_b + \lambda_c\right) \quad (4)$$

Where β is the sum of rotational speed ωt and current space phasor (vector) angle θ. The stator current is assumed to be sinusoidal, the zero sequence component of the current becomes zero and can be neglected. The current vector angle can be calculated accordingly using

$$\theta = \angle I_S = \tan^{-1}\left(\frac{i_q}{i_d}\right) \quad (5)$$

Here I_S is the stator current space phasor, i_d and i_q are the d-and q-axis currents. Even though the flux linkages have harmonic content, it is of such nature that the zero sequence flux linkage

component λ_o can be neglected and the sum of the linkages λ_d, λ_q, λ_o is approxiatly zero [20].

The flux linkages in both machine variables and rotating reference frame as functions of rotor position are shown in Fig.7 (a) and (b) respectively. The Finite Element Analysis (FEA) was performed at current vector angle of 45° elect, i_q= 8.485 A and i_d = 8.485 A. The three-phase windings are made of distributed double layer chorded coils to produce a sinusoidal inductance-position curve. Therefore, all the flux linkage waveforms are nearly an exact sinusoidal due to the sinusoidal excitation current.
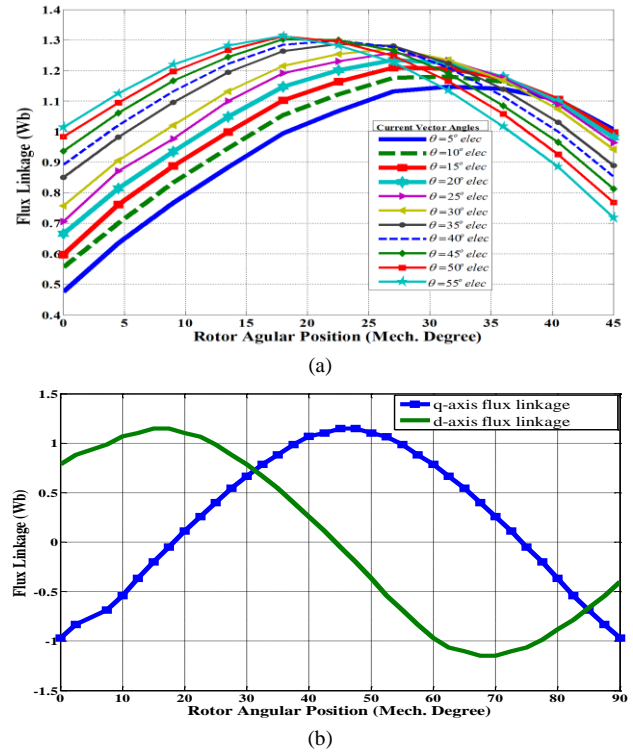

(a)

(b)

Fig.7: Flux-linkages as function of rotor position, (a), flux linkage of phase A for different current vector angle, (b) d-and q-axis flux linkages at current vector angle of 55^0 elec

D. Magnetic force distribution

The rotor surface and adjacent region i.e. airgap should have a fine finite element mesh since the Maxwell stress tensor method for force calculation is sensitive to mesh. Fig. 8 (a) shows the novel rotor within a closed surface Σ to be used for integration of Maxwell tensor, while Figs. 8 (b) and (c) give force density distribution on the rotor surface of the Novel SynRM and the Standard SynRM1 respectively. The resultant magnetic field force acting upon the object found within a closed surface is calculated by integrating the Maxwell stress tensor as [16], [21]

$$\overline{F} = \oint d\overline{F} = \mu_o \oint_{\Sigma}\left((\overline{H} \bullet \overline{N})\overline{H} - 0.5H^2\overline{N}\right)ds \quad (6)$$

The normal component of the stress tensor is a pressure force per unit area and does not contribute to overall torque. However, the tangential component is a shearing force per unit

area and contribute to the torque [22]. In electrical machines, it is convenient to choose the cylindrical surface in the middle of the airgap as the Maxwell integration surface [22].
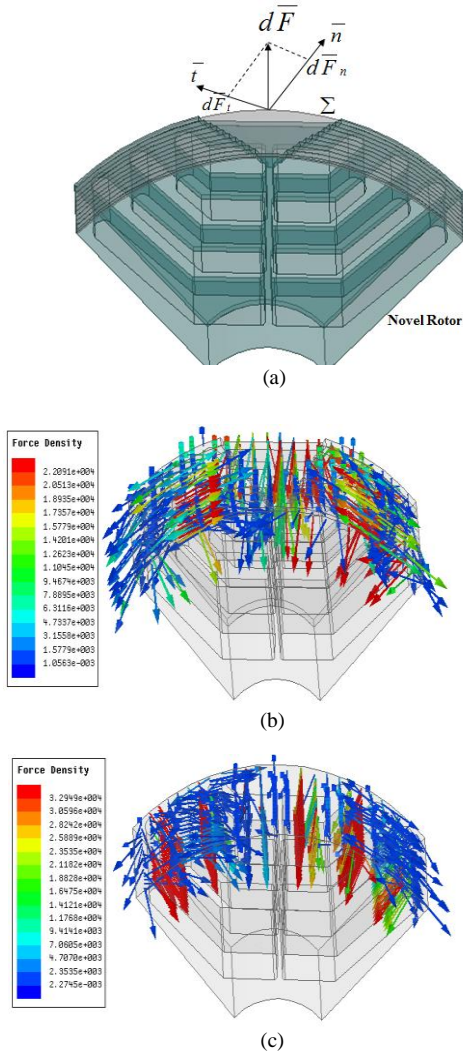

(a)

(b)

(c)

Fig. 8: (a) Novel rotor within a closed surface, (b) Novel SynRM force density distribution, (c) Standard SynRM1 force density distribution

Where *N* is the normal vector to the rotor surface. The tangential and normal forces to the surface per unit area are respectively calculated using [16]

$$dF_t = \mu_o\, H_t\, H_n ds \qquad (7)$$

$$dF_n = 0.5\mu_o\left(H_n^2 - H_t^2\right) ds \qquad (8)$$

The surface force density distribution on the rotor surface at full-load operation shown in Fig. 8 (b) and (c) was determined for a 3D field analysis.

E. Electromagnetic torque Analysis

The Novel SynRM average torque and torque ripple factors profiles as functions of current vector angle *θ*, for different stator currents are given in Fig. 9 (a) and Fig.9 (b) respectively.

Similar profiles are shown in Fig. 9 (c) and Fig. (d) for the Standard SynRM1.

(a)

(b)

(c)

(d)
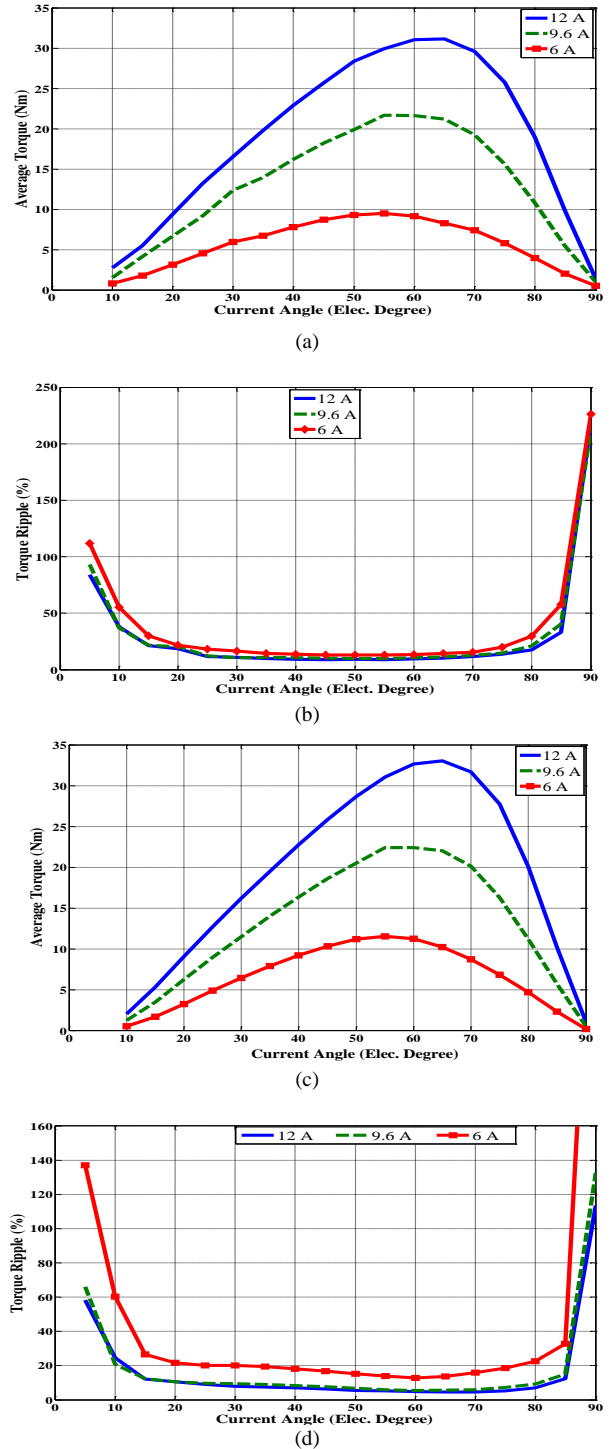
Fig. 9: Torque characteristics (a) average torque for Novel SynRM, (b) Torque ripple factor for Novel SynRM, (c) average torque for the Standard SynRM1, (d) Torque ripple factor for the Standard SynRM1

As noticed in the above FEA results, the torque is not maximized for $\theta = 45^o\ elec$ as expected. For the current of 9.6 A and 6 A, the average torque is maximized at the current vector angle of $55^o\ elec$. The current vector angle θ is shifted by $10^o\ elec$ with current of 12A and the average torque is

maximized at 65° *elec*. The shift of current angle from 55° to 65° *elec* in the Novel SynRM and Standard SynRMs is mainly due to saturation of radial and tangential bridges.

IV. PRACTICAL VALIDATION

A. Experimental Set-up

The experimental setting mainly comprises of the Novel three-phase SynRM coupled to a Wirbelstrombremse Siemens Eddy Current brake. The shaft torque, speed and mechanical power are measured by the rotary Magtrol's Model 3410 torque transducer with range from 0 to 50 Nm and a maximum speed of 4000 r/min. The torque transducer powers the torque meter and utilizes high speed Digital Signal Processing (DSP) to display torque, speed and mechanical power. The Dranetz PowerVisa 4400 three-phase power analyzer, equipped with eight independent channels, is utilized for advanced power monitoring and storage. The Tektronix TPS 2024 four channels digital oscilloscope is used to analyse both electrical and mechanical parameters of interest. The SynRM is started by means of an industrial drive of ACS880 type. Fig.10 shows the experimental setup rig photo.
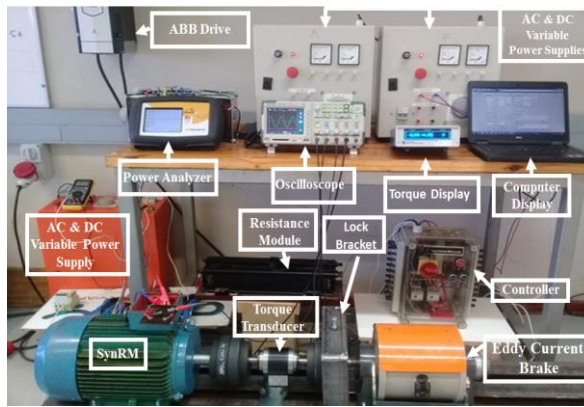

Fig. 10: Experimental setup rig photo

B. Machines Parameters and Performance Indexes

Table 2 compares the Novel and standard SynRM1 *d-* and *q-*axis magnetizing inductances and reactances, while table 3 compares the FEA and measured results of the saliency ratios "ζ", apparent maximum power factors "APFmax" as well as the airgap flux density angles "$\delta|_{maxAPF}$" and field weakening ratio "$K|_{maxAPF}$" at maximum power factor with a current vector angle of 20° *elec*.

Observing from Table 3, it is evident that the Standard SynRM1 has a higher saliency ratio at rated current and achieved an apparent maximum power factor of 0.712, on other hand the Novel SynRM has a higher *d-*and *q-*axis inductances difference "ΔL" which provides a higher average torque with a current vector angle of 20° *elec*.

During the standstill dc test, the torque was recorded at nine different positions from 10° to 90° *elec*. The average torque profiles as function of current vector angle for different currents are shown in Fig. 11 (a) for the Novel SynRM and in Fig. 11 (b) for Standard SynRM1, while Fig. 12 (a) compares the

average torque as function of magnetizing current when the SynRMs operate with a current vector angle of 20° *elec*. Fig 12 (b) illustrates the power factor and efficiency as function of load currents for both Novel SynRM and Standard SynRM1.

TABLE II
COMPARISON OF MAGNETIZING INDUCTANCE AND REACTANCE

Description	Novel SynRM		Standard SynRM1	
	FEA	Measured	FEA	Measured
L_{md} (mH)	57.85	46.56	38.92	34.30
L_{mq} (mH)	11.35	9.60	6.78	6.10
X_{md} (Ω)	18.17	14.62	12.22	10.77
X_{mq} (Ω)	3.56	3.01	3.83	1.91

TABLE III
COMPARISON OF INDEXES AT CURRENT ANGLE OF 20° *ELEC*

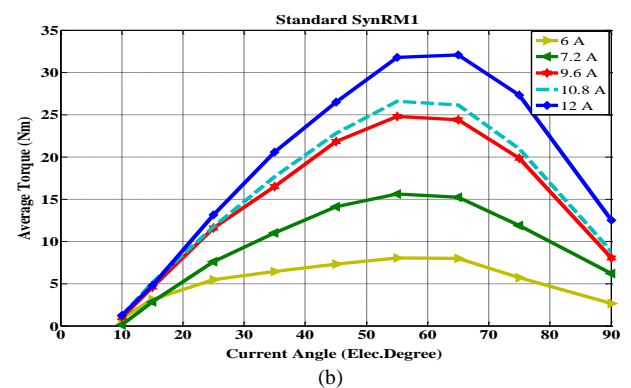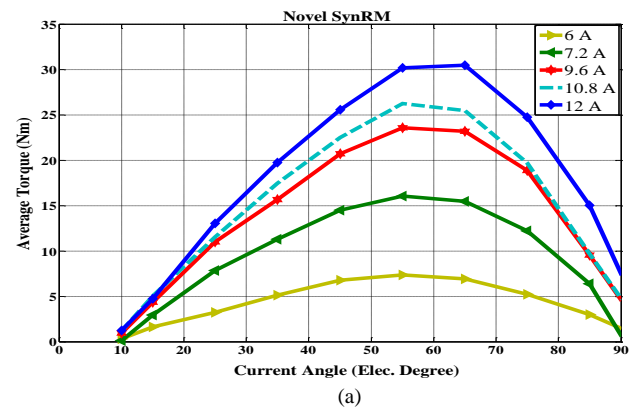| Description	Novel SynRM		Standard SynRM1	
	FEA	Measured	FEA	Measured
ΔL (mH)	46.51	36.96	32.14	28.20
ζ	5.10	4.85	5.74	5.62
T_{av} (Nm)	10.46	9.80	8.75	7.30
APF_{max}	0.672	0.658	0.703	0.698
$\delta|_{maxAPF}$	4.3^o *elec*	3.8^o *elec*	3.6^o *elec*	3.5^o *elec*
$K|_{maxAPF}$	1.35	1.29	1.41	1.37

(a)

(b)

Fig. 11: Measured average torque as function of current angle, (a) Novel SynRM, (b) Standard SynRM1
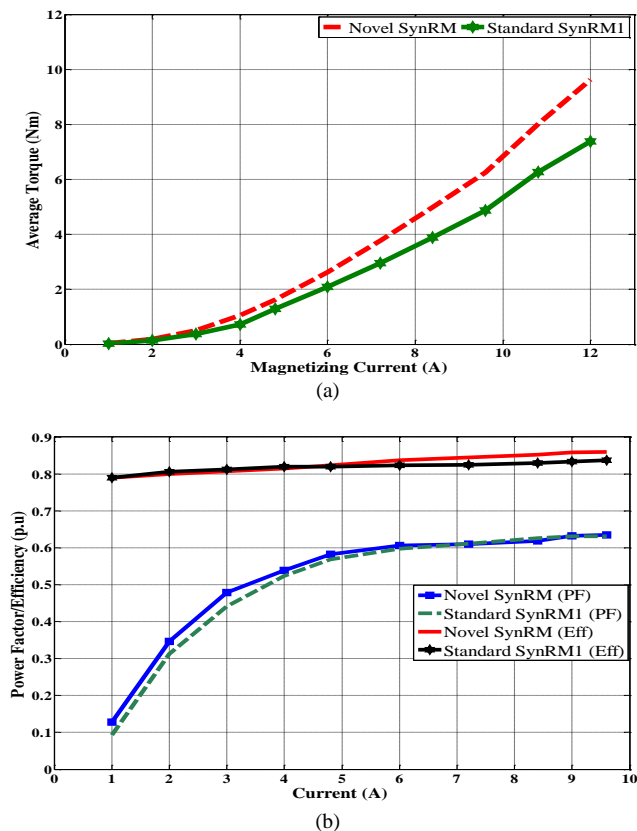
(a)

(b)

Fig. 12: Comparison between the Novel SynRM Standard SynRM1, (a) and Average as function of magnetizing current, (b) power factor and efficiency as a function of load currents

From observing Figs. 11 (a) and (b), it is noticed that for a current of 6 A, 7.2 A, 9.6 A and 10.8 A, the average torque is maximized at current angle of 55º *elec* for both Novel SynRM and Standard SynRM1. Once the maximum current of 12 A is applied, the current angle shifts for a value of 10º *elec* and the average torque is maximized at 65º *elec*. The FEA results discussed in section III have shown similar behaviors as the measured results illustrated in Fig. 11. The magnetic saturation of thin tangential and radial bridges in both Novel SynRM and Standard SynRM1 has caused the current to quickly shift from 45º *elec* even when less current is applied. The thin radial ribs are heavily saturated by the *q*-axis MMF in the Novel machine than in the Standard SynRM1. For a small current angle of 20º *elec*, the Novel SynRM generates high torque density due to injection of the 3rd harmonics caused by saturation.

With the absence of rotor copper loss, the SynRM has a high efficiency compared to the induction motor. On the other hand, the power factor in the SynRMs depends on the saliency ratio. A greater saliency ratio will provide a good power factor. The measured power factor and efficiency shown in Fig. 12 (b) were obtained at rated speed and rated voltage. Observing from Fig. 12 (b), it is evident that the power factor is very low when both SynRMs run on light load. The power factor in both SynRMs reaches about 0.63 for a current of 9.6 A, which corresponds to 80 % of the rated condition. It is also noted that between the load currents of 1 A and 4 A, the Novel SynRM has a higher power factor than the Standard SynRM1. This slight advantage is attributed to the fact the Novel SynRM has a high saliency ratio in the region that lies between 1 A and

4 A. The measured results depicted in Fig.12 (b) also indicate that the efficiency of both SynRMs is good. The novel SynRM has better efficiency than the Standard SynRM1 at a bigger load current. The upper hand is attributed to the fact that the Novel SynRM has less iron on the rotor due to lamination cu-offs on the *q*-axis. The Novel SynRM has total iron loss of 618.32 W, while its counterpart, Standard SynRM1, is found to have 733.22 W, when both motors are operating at 80 % of rated condition.

V. CONCLUSION

This paper has presented the evaluation of key performance indexes of the novel synchronous reluctance motor having a sinusoidal rotor lamination shape in the axial direction. In the FEA, the magnetic flux was not calculated for unit depth and multiply by the stack length to find the actual magnetic flux in the machine, as it always the case in electric machines with plane symmetry. The actual magnetic flux was obtained by employing the superposition principle. Through FEA results, the Novel SynRM has proved to have the edge to produce high torque density with lesser ripple factor as compared to the Standard SynRM. The validation of FEA results has been carried out through practical measurements, and both methods have shown a good correlation. To conclude, the novel synchronous reluctance motor with sinusoidal anisotropic rotor is seen to be a strong contender in AC drives that require high torque density, lower ripple contents and high efficiency. The absence of a permanent magnet on the rotor makes the novel motor to be cheaper than the popular permanent magnet synchronous reluctance machine.

REFERENCES

[1] W. Wang and B. Fahini, "*Comparative study of Electric Drives for EV/HEV propulsion system*", IEEE 2012 Electrical System for Aircraft, Railway and Ship Propulsion (ESARS), 16-18 Oct. 2012, Bologna, Italy

[2] V. Croitorescu, I. Croitorescu and G Danciu, "Functional modelling of an electric machine used on road vehicles", 8th International Symposium on advanced topics in electrical engineering, May 23-24, 2013, Bucharest, Rumania.

[3] F. N. Jurca, R. Mircea, C. Martis, R. Martis and P. P. Florin, " Synchronous reluctance motors for small electric traction vehicle", 2014 International Conference and Exposition on Electrical and Power Engineering (EPE 2014), 16-18 October, Iasi, Romania.

[4] J. Lin, K. W. E. Cheng, Z. Zhang and X. Xue, "Experimental investigation of in-wheel reluctance motor driving system for future electric vehicles", 3rd International conference on Power Electronics Systems and Applications, 2009.

[5] S. Taghavi and P. Pillay, "A mechanically robust rotor with transverse-laminations for a synchronous reluctance machine for traction applications", 2014.

[6] N. Bianchi, S. Bolognani, D. Bon, and M. D. Pre', Rotor Flux-barrier Design for Torque Ripple Reduction in Synchronous Reluctance and PM-Assisted Synchronous Reluctance Motors. IEEE Trans. on Ind. Appl., vol. 45, Issue 3, May-June 2009, pp. 921-928.

[7] N. Bianchi, S. Bolognani, D. Bond and M. D. Pre', Rotor Flux-barrier Design for Torque Ripple Reduction in Synchronous Reluctance Motors. *Proc. 41th IEEE Conf. On Industry Applications*, 2006, 1193-1200.

[8] E.C Lovelace, "Optimization of a magnetically saturable IPM Sync. Mac. Drive", PhD, Dept. of Elec. Eng. & Comp. Sci., MIT, 2000.

[9] R. R. Fessler and M. Olszewski. "*Assessment of Motor Technologies for Traction Drives of Hybrid and Electrical Vehicles*", USA Department of Energy, FreedomCar and Vehicle Technologies Mar 2011.

[10] N. Bianchi and S. Bolognani, A Consoli, T. M. Jahns, R. D. Lorenz, E. C. Lovelace, S. Morimoto and A. Vagati, "Design Analysis and Control of Interior Permanent Magnet Synchronous Machines". *Proceeding of*

International Conference on Electrical Machines, ICEM. Aug. Helsinki, 2000.

[11] E. Armando, P. Guglielmi, G. Pellegrino, M. Pastorelli and A. Vagati, "Accurate Modelling and Perf. Anal. of IPM-PMASR Motors". *IEEE Trans. on Ind. Appl.*, vol. 45, Issue 1, Jan-Feb 2009, pp. 123-130.

[12] M. J Kamper, F. S. Van der Merwe and S. Williamson, "Direct finite element design optimization of the cage-less reluctance synchronous machine", *IEEE Trans. on Energy Con.*, Vol. 11, IS, 3, Sept. 1996, pp: 547-555.

[13] M. Sanada, K. Hiramato, S. Morinoto, and Y. Takeda. "Torque Ripple Improvement for Synchronous Reluctance Motor Using Asymmetric Flux Barrier Arrangement". *Proc. IEEE Ind. App. Soc. Annual Meeting*, 12-16 Oct. 2003.

[14] W. Zhao, T. A Lipo and B. Kwon "Material-efficiency magnet shape for torque pulsation minimization in synchronous permanent motors". *IEEE Trans. On Industrial Electronics*, vol. 61, Issue 10, 2014, pp. 5579-5787.

[15] M. Muteba, B. Twala and D. Nicolae "Torque Ripple Minimization in Synchronous Reluctance Motor Using a Sinusoidal Rotor Lamination Shape", *Proc. of the Int. Conf. on Elect. Machines*, ICEM, 2016, Sep 4-7, 2016, Lausanne, Switzerland.

[16] I. Boldea and L. Tutelea, "Electric Machines: Steady State, Transients and Design with Matlab", *Taylor and Francis*, 2010.

[17] M.V. Ferreira da Luz, E. Deschamps, F. Runcos and S.L. Nau, Analysis of 65 kVA high efficiency synchronous generator using finite element Method", *Proc. of the XII Int. Sym. on Electromagnetic Fields in Mechatronics,* Electrical and Electronic Engineering (ISEF), Spain, 2005.

[18] M. Muteba, B. Twala and D. Nicolae "Based 3D Finite Element Analysis of a Synchronous Reluctance Motor with Sinusoidal Rotor Lamination Shape", *Proc. of the Int. Conf. on Elect. Machines*, ICEM, 2016, Sep 4-7, 2016, Lausanne, Switzerland.

[19] V. Bilyi, D. Gerling and D. Bilyi, "*Flux barrier design method for torque ripple reduction in synchronous reluctance machines*". Busan, Korea, *IEEE* Transportation Electrification Conference and Expo, Asia- Pacific (ITEC), June 1-4, 2016.

[20] A. Fratta, G. P. Troglia, A. Vagati, and F. Villata, "Evaluation of torque ripple in high performance synchronous reluctance motors*".*, *IEEE Industry Application Society Annual Meeting*. Toronto, Canada, 1993.

[21] L. Vandevedle and Melkebeek, A. A., "A survey on magnetic force distribution based on different magnetization models and on virtual work principle". *IEEE Transaction on Magnetics,* 37(5), pp. 3405-3409, 2001

[22] Y. G. Guo and J. G. Zhu, "Improved methods for force and torque calculation in electrical machines by 3D finite element analysis". *Proceedings on the 5th International Conference on Electrical Machines and Systems*, Chenyang, China, 2001